Application of shell elements to buckling-analysis of thin-walled somposite laminated beams

Application of Shell elements to buckling-analyses of thin-walled composite laminates

B.A. Göttgens

MT 12.02

Internship report

Coach: Dr. R. E. Erkmen

University of Technology Sydney
Department of Civil Engineering

Supervisor: Prof. Dr. M.G.D Geers

Technische Universiteit Eindhoven
Department of Mechanical Engineering
Division of Computational and Experimental mechanics

December 15, 2011 Eindhoven

Contents

1 Introduction

Fibre-reinforced polymer laminas are formed by embedding continuous fibres in a resin matrix, which binds the fibres together forming a composite ply. The plies are then stacked together in a certain sequence[1] to form composite-laminated plates (figure 1). The use of fibre-reinforced polymer laminas as a construction material has increased in recent years. The primary reason for this increase is their non-corrosive nature and long term durability, high tensile strength-to-weight ratio, electromagnetic neutrality and resistance to chemical attack. Because of their high strength to weight ratios slender structural components may be formed by using composite laminates due to which, however, *buckling may become a main concern*, and fibre orientation and boundary conditions of the laminated plates are important parameters determining the buckling behaviour.

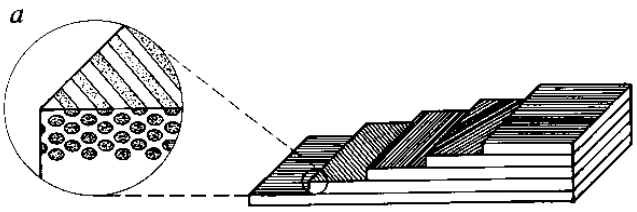

figure 1: structure of a composite laminated plate

Numerous theories have been proposed to date to describe the kinematics and stress states of thin-walled composite laminated structures. However, closed form-analytical solutions considering all aspects of the composite laminated structure buckling behaviour are not always available and therefore, in this study a numerical tool that captures the buckling behaviour of composite laminated structures has been developed.

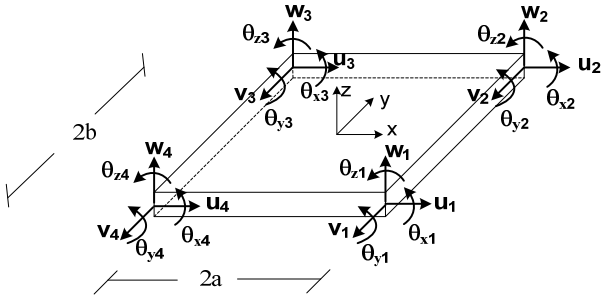

figure 2: Four node flat rectangular shell element with six degrees of freedom at each corner

Most commercially available software calculate structures that are constructed of thin-walled beams based on simple beam theory (figure 5) which assumes lateral buckling behaviour (the cross-section of the beam remains constant) and thus can only capture global (lateral) beam buckling effects. The numerical tool uses a shell-type finite element formulation in order to capture local buckling effects (figure 3). The shell elements are applied as a superposition of a

four node rectangular plate with a four node rectangular membrane with six degrees of freedom per node (figure 2).

When local buckling effects occur (figure 3), the critical buckling load decreases dramatically. As buckling may become a main concern in slender structural components made of composite laminates, capturing these local effects is very important.

figure 3: flange buckling of an I-shaped beam, a local buckling effect

Usually, flanges are welded or bolted on the sides of thin walled metal beams in order to prevent local buckling (figure 4). Applying this solution to composite laminated thin-walled beams is not a valid option, because after the material is cured, adding material is very difficult and drilling bolt-holes can cause delamination. Therefore with regard to composite laminated structures it is *very* important to determine the critical buckling load accurately in the design phase of the structure.

figure 4: flanges applied to prevent local buckling effects

For the used kinematic assumptions and the finite element formulation please refer to the published article that was the result of these studies [2]. A complete understanding of the applied kinematics and finite element formulation were not considered essential, regarding the time span

of the internship. They are not included in this report for the sake of errors or misinterpretations on the part of the student.

Recently a new framework for the development of thin plate finite elements called “the twist Kirchhoff theory” was introduced by Brezzi, Evans, Hughes and Marini [2]. A family of rectangular plate elements was presented in the publishing and apparently these elements have a very high convergence rate.

The goal of the studies was twofold:

- Developing a numerical tool that could capture any buckling behavior of thin walled composite laminated structures
- Performing convergence studies on the twist-Kirchhoff theory based elements by applying them to cases regarding composite laminated plates

In order to convince others that the numerical tool provides correct results a series of cases were compared to well known closed form solutions as described in chapter two. Chapter three discusses parametric case studies that illustrate the influence of laminate layup and the transition from global to local buckling behavior, depending on several parameters. Chapter four compares convergence studies of four-node shell elements with the twist-Kirchhoff theory based shell elements. In chapter five conclusions about the studies are drawn.

[1] A laminate stacking sequence is denoted by $[\theta_1/\theta_2/\ldots/\theta_n]_{xs}$ where $\theta_1 - \theta_n$ denote the angles of layers 1 to n respectively in degrees, $[..]_x$ denotes how many times the stacking sequence is repeated and $[..]_s$ denotes whether or not the stacking sequence is mirrored about the lamina mid-plane.

2 Validation of the numerical tool

Prior to convergence and parametric case studies, the tool was validated by comparing several cases to well known closed form solutions.

2.1 One-dimensional beam buckling

Starting off simply, a one-dimensional beam buckling case was modeled and compared to an analytical solution. Both isotropic and composite laminated material properties were investigated.

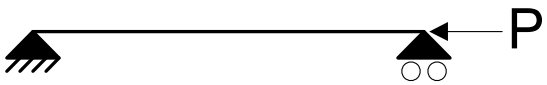

figure 5: one-dimensional beam buckling

2.1.1 Case description

A doubly hinged beam of length 100, of width 1 and height 1 under a compressive load *P* was chosen for this case (figure 5). Six different cases were distinguished to test the code as can be seen in table 1. Case 1 considers an isotropic beam. Cases 2 to 5 consider different layups of composite laminated beams.

table 1: case descriptions

Case no.	Material properties	Layup
1	isotropic	-
2	composite laminated	[0]
3	composite laminated	[90]
4	composite laminated	$[0/90]_s$
5	composite laminated	$[0/45/90/-45]_s$
6	composite laminated	[0 45 -45 90]s

Material properties were chosen according to table 2. Subscripts 1 and 2 denote the principal directions in the local coordinate system of a laminate ply.

table 2: material properties

Case	E_1	E_2	G_{12}	G_{13}	G_{23}	ν_{12}	ν_{21}
isotropic	1	1	0.1	0.1	0.1	0.25	0.25
composite	1	$\frac{E_1}{5}$	$\frac{E_2}{2}$	$\frac{E_2}{2}$	$\frac{E_2}{5}$	0.25	$\frac{E_2}{E_1}\nu_{12}$

2.1.2 Mesh generation

To capture one-dimensional beam behavior with shell elements, a mesh of 100 by 1 square elements was generated and the nodes were numbered according to figure 6 below. Each element has length 1 and is assigned a thickness-value of 1.

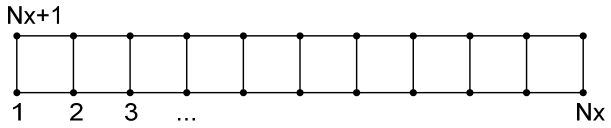

figure 6: node numbering for one-dimensional beam model

2.1.3 Boundary conditions

In order to capture the boundary conditions as displayed in figure 5, nodes were constrained and forces were applied to nodes according to the red and green arrows shown in figure 7, respectively.

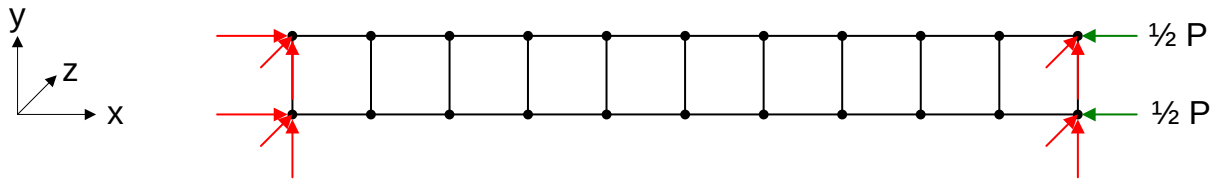

figure 7: applied boundary conditions

2.1.4 Closed form solutions

The following closed form solution was compared to the results of the numerical tool for the isotropic case.

$$P_{cr} = \frac{\pi^2 EI}{L^2} \tag{1}$$

where $E = E_1$. According to [3], in the case of cylindrical composite laminated plate buckling, the critical buckling force can be calculated according to

$$P_{cr} = D_{11}\frac{\pi^2}{a^2}\left(1 - \frac{B_{11}\bar{B} + B_{16}\bar{C}}{D_{11}A}\right) \tag{2}$$

where D_{11}, B_{11} and B_{16} are the corresponding elements of matrices B and D. $\bar{B}$ and $\bar{C}$ can be calculated according to:

$$\bar{B} = \frac{B}{A}, \qquad \bar{C} = \frac{C}{A}$$

$$A = A_{11}A_{66} - A_{16}A_{16}, \qquad B = B_{11}A_{66} - B_{16}A_{16}, \qquad C = A_{11}B_{16} - A_{16}B_{11}$$

where A_{ij} and B_{ij} are elements of matrices A and B. For the determination of extensional stiffness matrix A, coupling stiffness matrix B and bending stiffness matrix D please refer to appendix 1.

2.1.5 Results

All six cases were run with the numerical tool. The resulting values for the critical applied load were compared to the closed form solutions and are displayed in table 3 below.

table 3: resulting critical applied loads

Case no	Numerical tool	(3)	(4)
1	8.257E-05	8.22E-05 (0.0390)	8.773E-05 (0.06251)
2	8.257E-05	-	8.773E-05 (0.06251)
3	1.645E-05	-	1.666E-05 (0.01257)
4	7.427E-05	-	7.496E-06 (0.00926)
5	5.835E-05	-	6.100E-05 (0.04553)
6	5.865E-05	-	6..275E-05 (0.06996)

2.1.6 Remarks

Our case of simply supported one-dimensional beam buckling modeled by shell elements can be seen as a special case of cylindrical composite laminated plate buckling (figure 8). The outcomes of (1) and (2) did not match exactly however!

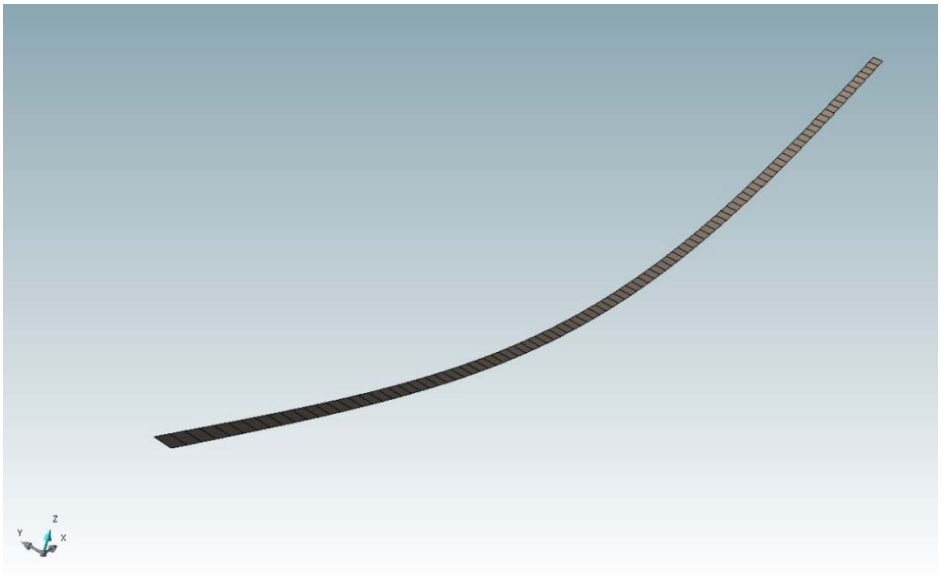

figure 8: buckled shape of the modeled beam

2.2 Plate deflections

After validating one-dimensional buckling cases, plate deflections were compared to closed form solutions prior to validating correct plate buckling behavior. Once again both isotropic and composite laminated materials were investigated.

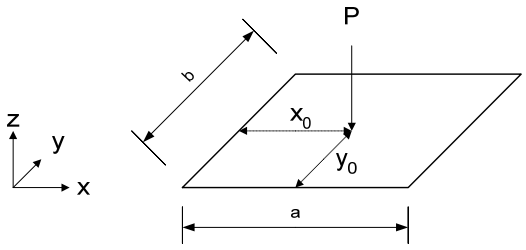

figure 9: a point load applied to a rectangular plate

2.2.1 Case description

A simply supported plate of length a, width b = 100 and thickness 1 under an applied point load P at the centre was chosen for this case (figure 9). Twelve different cases were distinguished to test the code as can be seen in table 4. Cases 1 to 5 consider mesh refinement of isotropic or composite laminated square plates. Cases 6 to 9 consider different layups of composite laminated square plates. Cases 10 to 12 consider non-square plates. Material properties were chosen according to table 2.

table 4: case descriptions

Case no.	Material properties	Layup	a	elements
1	isotropic	-	100	6 x 6
2	isotropic	-	100	15 x 15
3	composite laminated	[0]	100	6 x 6
4	composite laminated	[0]	100	15 x 15
5	composite laminated	[0]	100	20 x 20
6	composite laminated	[90]	100	6 x 6
7	composite laminated	[0 90]s	100	6 x 6
8	composite laminated	[0 45 90 -45]s	100	6 x 6
9	composite laminated	[0 45 -45 90]s	100	6 x 6
10	composite laminated	[0]	140	10 x 14
11	composite laminated	[0]	200	6 x 12
12	composite laminated	[0]	300	6 x 18

2.2.2 Mesh generation

Meshes were generated according to table 4 and nodes were numbered according to figure 10 below. Each element has an assigned a thickness-value of 1.

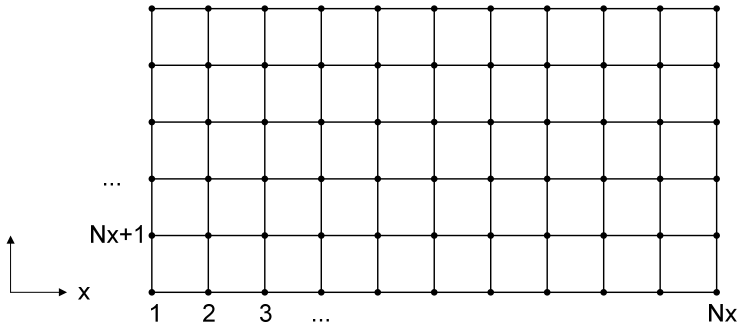

figure 10: node numbering of a rectangular plate

2.2.3 Boundary conditions

In order to capture the boundary conditions as displayed in figure 9, nodes were constrained and forces were applied to nodes according to the red and green arrows shown in figure 11figure 7, respectively.

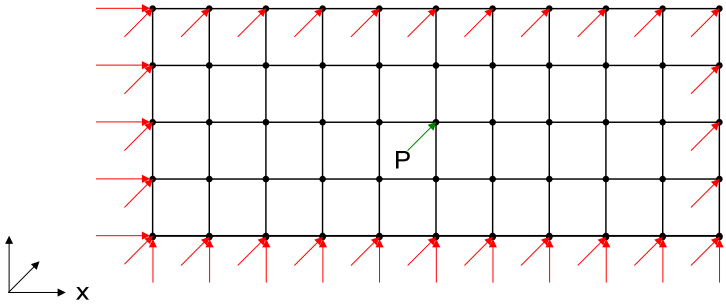

figure 11: applied boundary conditions

2.2.4 Closed form solutions

For a simply supported isotropic square plate under a central point load, according to [4], the maximum deflection of the plate can be described as:

$$\omega_0 = 0.0116\frac{Pa^2}{D} \tag{3}$$

where

$$D = \frac{Et^3}{12(1-\nu^2)}$$

For a simply supported composite laminated plate under a central point load, according to [5] the maximum displacement is given by

$$\omega_0 = \frac{Q_{mn}}{d_{mn}} \sin \alpha x_0 \sin \beta y_0 \tag{4}$$

where

$$Q_{mn} = \frac{4N}{ab} \sin \alpha x_0 \sin \beta y_0$$

$$d_{mn} = \left(\frac{\pi}{b}\right)^4 [D_1(ms)^4 + 2D_3(mns)^2 + D_2(n)^4]$$

Where s is the ratio of a over b (the aspect ratio). D_1, D_2 and D_3 represent elements D_{11}, D_{22} and combination of elements $(D_{12} + 2D_{66})$ from matrix D, respectively. Scalars α and β are defined as:

$$\alpha = \frac{m\pi}{a}, \qquad \beta = \frac{n\pi}{b}$$

Where m and n are defined as the modes of buckling in x- and y-directions, respectively.

2.2.5 Results

All twelve cases were run with the numerical tool. The resulting values for the critical applied load were compared to the closed form solutions and are displayed in table 5 below.

table 5: resulting maximum plate deflections

Case no.	Numerical tool	(3)	(4)
1	-1.870E+03	-1.305E+03 (0.3021)	-1.607E+03 (0.1407)
2	-1.720E+03	-1.305E+03 (0.2413)	-1.607E+03 (0.0658)
3	-3.48E+03	-	-2.87E+03 (0.1751)
4	-3.19E+03	-	-2.87E+03 (0.1000)
5	-3.34E+03	-	-2.87E+03 (0.1405)
6	-3.48E+03	-	-2.87E+03 (0.1751)
7	-3.40E+03	-	-2.87E+03 (0.1556)
8	-3.08E+03	-	-2.54E+03 (0.1751)
9	-2.96E+03	-	-2.46E+03 (0.1703)
10	-3.49E+03	-	-2.66E+03 (0.2366)
11	-3.54E+03	-	-2.14E+03 (0.3951)
12	-3.54E+03	-	-1.53E+03 (0.5667)

2.2.6 Remarks

Cases 10 to 12, which consider non-square plates differ quite much (unacceptably) from the closed form solution. Whether the error resides in the numerical tool or the closed form solution remains unclear. However, for all other validation cases the tool proved to be correct.

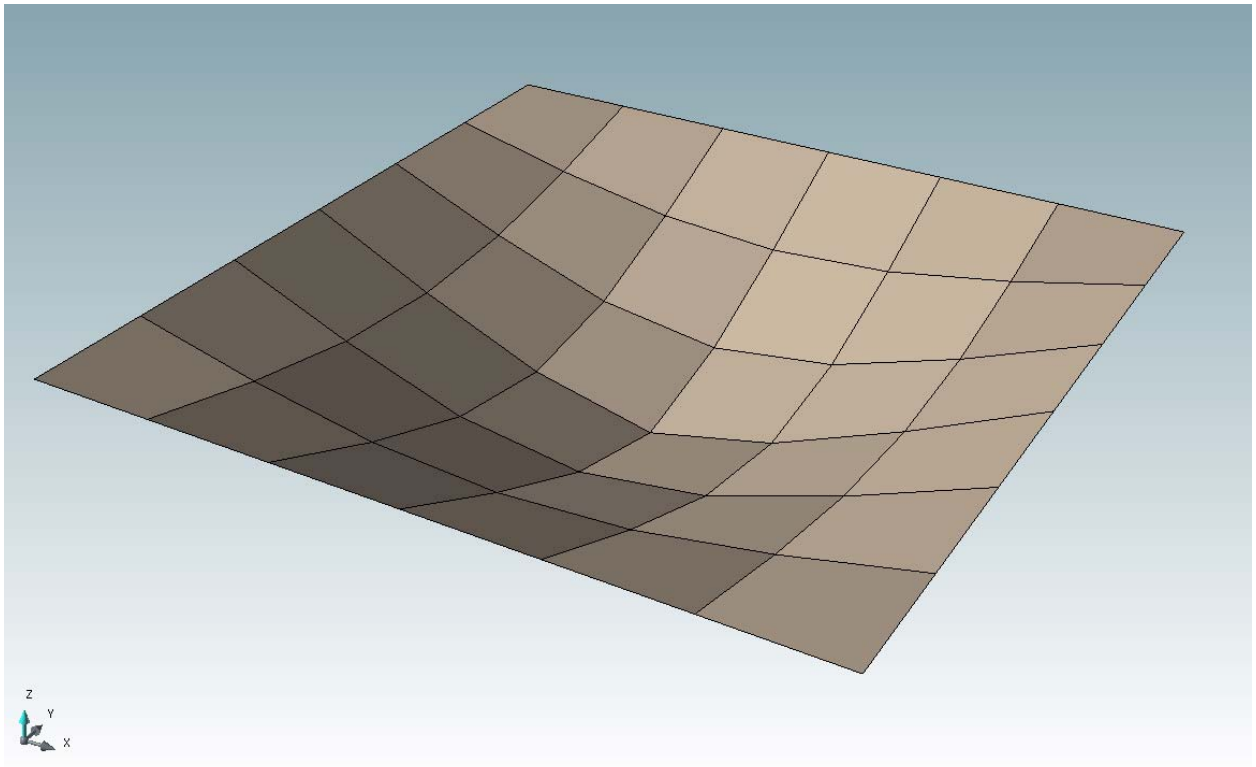

figure 12: deflected shape of the modeled plate

2.3 Plate buckling

After determining that the numerical tool can provide correct results concerning plate deflections, closed form solutions concerning plate buckling behavior were compared to the results of the numerical tool. Only composite laminated materials were used in this case.

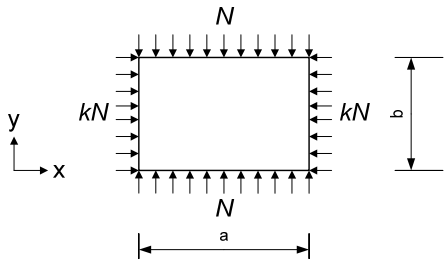

figure 13: biaxial compressive loading applied to a rectangular plate

2.3.1 Case description

A simply supported plate of length a, width b = 100 and thickness 1 under an applied biaxial load N_x and N_y was chosen for this case. The ration of N_y over N_x is defined as κ (figure 13). Eleven different cases were distinguished to test the code as can be seen in table 4. Cases 1 to 4 consider different values of κ. Cases 5 to 9 consider different layups of composite laminated square plates. Cases 10 and 11 consider non-square plates. Material properties were chosen according to table 2.

table 6: case descriptions

Case no.	κ	Layup	a	elements
1	1.00	[0]	100	6 x 6
2	0.75	[0]	100	6 x 6
3	0.50	[0]	100	6 x 6
4	0.25	[0]	100	6 x 6
5	0.50	[0]	100	6 x 6
6	0.50	[90]	100	6 x 6
7	0.50	[0 90]s	100	6 x 6
8	0.50	[0 45 90 -45]s	100	6 x 6
9	0.50	[0 45 -45 90]s	100	6 x 6
10	0.50	[0]	200	6 x 12
11	0.50	[0]	300	6 x 18

2.3.2 Mesh generation

Meshes were generated according to table 4 and nodes were numbered according to figure 10. Each element has an assigned a thickness-value of 1.

2.3.3 Boundary conditions

In order to capture the boundary conditions as displayed in figure 13, nodes were constrained and forces were applied to nodes according to the red and green arrows shown in figure 14figure 7, respectively.

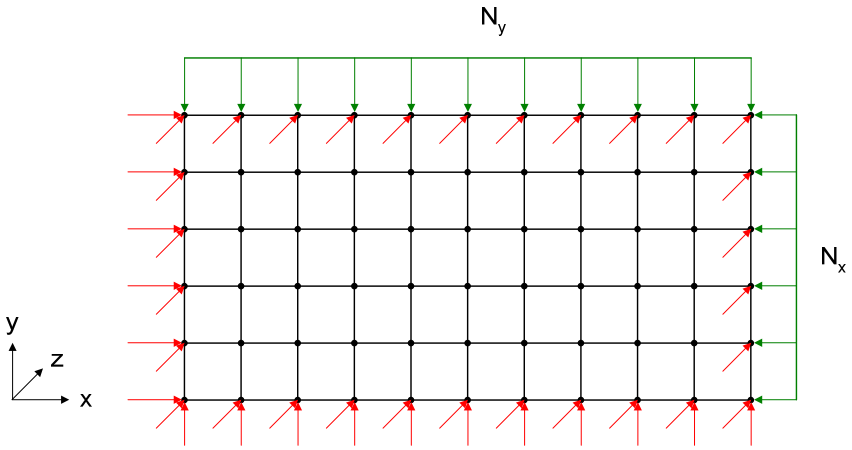

figure 14: applied boundary conditions

2.3.4 Closed form solution

According to [5] in the case of a simply supported rectangular composite laminated plate, the critical buckling load may be expressed as

$$N_{cr} = -\frac{[D_1\alpha^4 + 2D_3\alpha^2\beta^2 + D_2\beta^4]}{\kappa\alpha^2 + \beta^2} \tag{5}$$

where κ is the ratio of $N_y$over N_x. This solution is *only* valid in the case of balanced symmetrical layups, meaning that the layup is symmetrical about the mid-plane and that for every layer of fiber-orientation θ above the mid-plane, there is a layer of fibre-orientation $-\theta$ below the mid-plane.

2.3.5 Results

All eleven cases were run with the numerical tool. The resulting values for the critical applied load were compared to the closed form solutions and are displayed in table 7table 5 below.

table 7: resulting critical buckling loads

Case no.	Numerical tool	(5)
1	7.6156E-03	7.0586E-03 (0.07313)
2	6.5424E-03	6.0503E-03 (0.07523)
3	5.1025E-03	4.7058E-03 (0.07776)
4	3.0722E-03	2.8235E-03 (0.08097)
5	5.1025E-03	4.7058E-03 (0.07776)
6	5.0433E-03	4.7058E-03 (0.06694)
7	5.1031E-03	4.7058E-03 (0.04083)
8	5.5437E-03	5.3174E-03 (0.05375)
9	5.8133E-03	5.5009E-03 (0.07313)
10	7.4307E-03	4.2060E-03 (0.43396)
11	7.4307E-03	4.1719E-03 (0.52629)

2.3.6 Remarks

Once again, cases 10 and 11, which consider non-square plates differ quite much (unacceptably) from the closed form solution. However in the case of plate buckling the difference can be explained because the closed form solution assumes the buckled shape to be formed by perfect half-sine-waves whereas the numerical tool calculates a different kind of sine-wave as can be seen in figure 15. This kind of resulting buckled shape for plates is explained by [6].

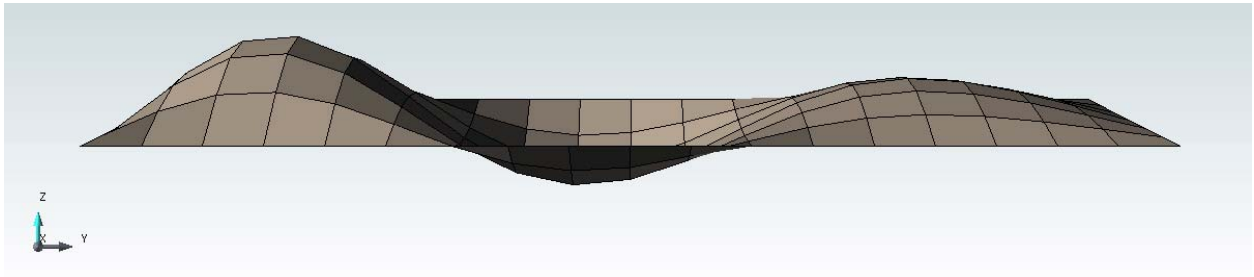

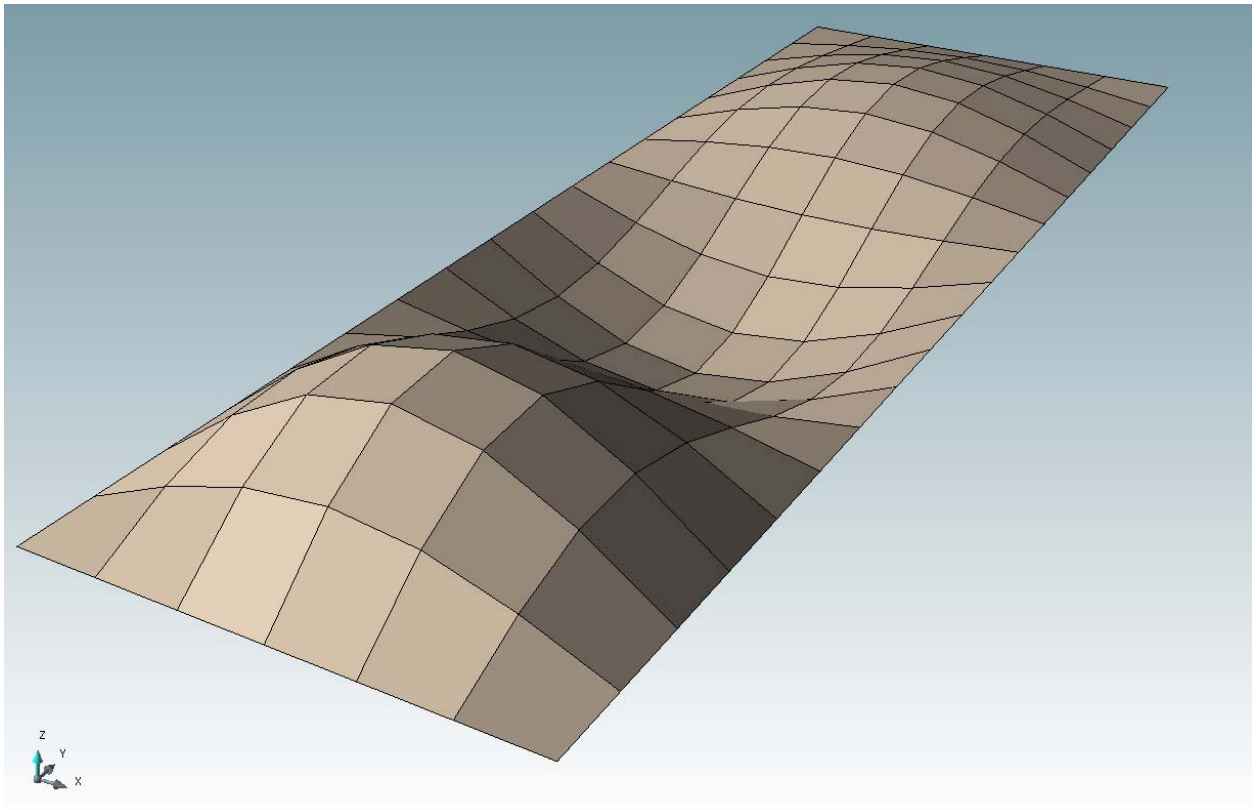

figure 15: buckled shape of a non-square plate

2.4 One-dimensional thin-walled beam buckling

After determining that the numerical tool can provide correct results concerning deflections and buckling behavior of plates, the tool was modified to determine the buckling behavior of thin-walled beams of any arbitrary cross section. First, in order to gain confidence an isotropic I-shaped beam was allowed to buckle in a one-dimensional way (no torsional buckling was allowed) and compared to (1). Then in section 2.5 several cases of isotropic and composite laminated I-shaped beams under various boundary conditions ware compared to their respective closed form solutions.

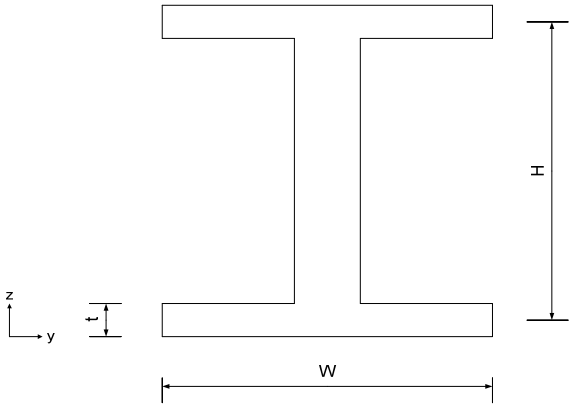

figure 16: dimensions of an I-shaped beam

2.4.1 Case description

A doubly hinged I-shaped beam of length 4000, width 200, height 200 and thickness 24 (figure 16) under a compressive load (figure 5) was chosen for this case. Material properties were chosen according to table 8. Two different cases were distinguished to test the code. Case 1 considers the beam to buckle over the z-axis (figure 20), case 2 considers the beam to buckle over the y-axis (figure 21).

table 8: material properties

E_1	E_2	G_{12}	G_{13}	G_{23}	ν_{12}	ν_{21}
200000	200000	80000	80000	80000	0.25	0.25

2.4.2 Mesh generation

Nodes were numbered according to figure 17 and then continued along the x-axis for every 200 units of length, in order to create square elements.

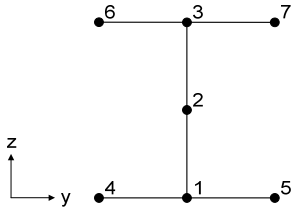

figure 17: node numbering of an I-shaped beam section

Then nodes were allocated to the elements. Nodes could be allocated in four different ways (figure 18) but in the end seemed to have no effect on the results. For this case clockwise 1 node allocation was chosen (figure 18).

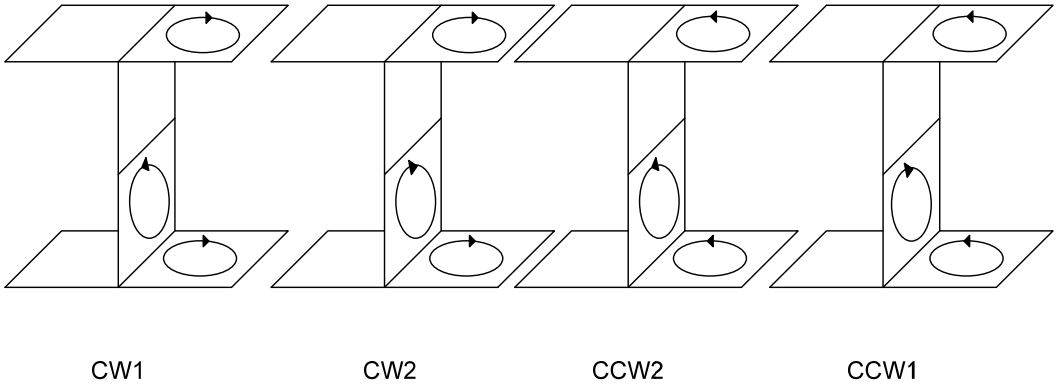

figure 18: node allocation to the elements

2.4.3 Boundary conditions

In order to capture the boundary conditions as displayed in figure 5, nodes were constrained and forces were applied to nodes according to the red and green arrows shown in figure 19figure 7, respectively. The left figure shows constraints applied to the left end of the beam, the right picture shows constraints and applied forces to the right end of the beam.

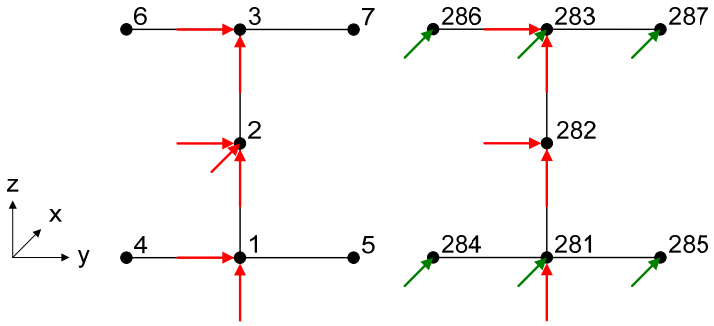

figure 19: aplied boundary conditions to the left and right ends of the beam

2.4.4 Closed form solution

To compare the critical buckling force, (1) was used. For the case where the beam was allowed to hinge freely over the y-axis, I was chosen the moment of inertia over the y-axis. For the case where the beam was allowed to hinge freely over the z-axis, I was chosen the moment of inertia over the z-axis.

2.4.5 Results

Both cases were run with the numerical tool. The resulting values for the critical applied load were compared to the closed form solutions and are displayed in table 9 below.

table 9: resulting critical buckling loads

Case	Numerical tool	(1)
1)	4.021E+06	3.973E+06 (0.0120)
2)	1.327E+07	1.325E+07 (0.0020)

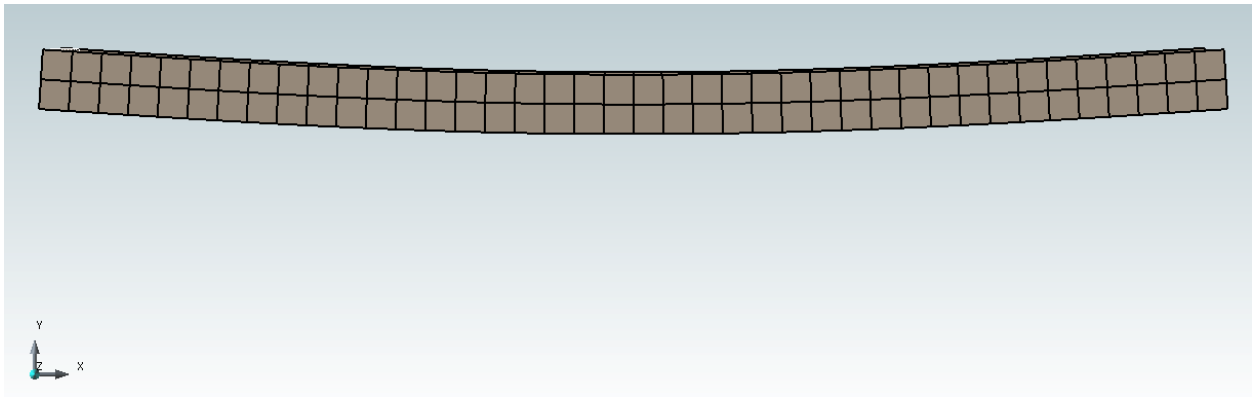

figure 20: buckled shape of the I-beam buckled over the z-axis (case 1)

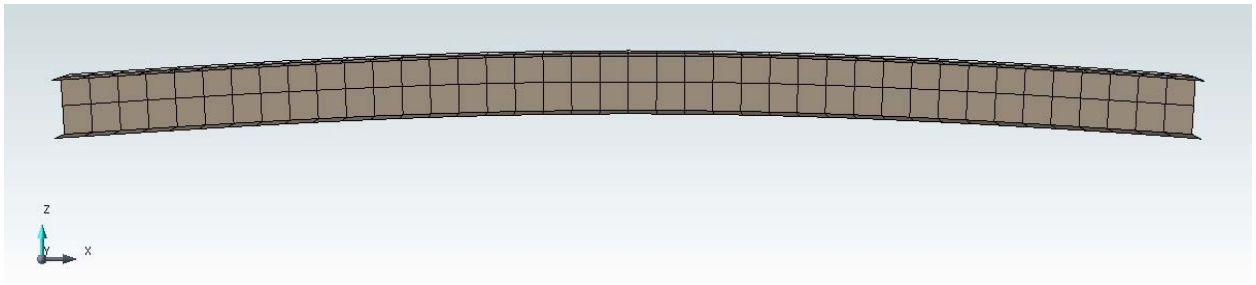

figure 21: buckled shape of the I-beam buckled over the y-axis (case 2)

2.4.6 Remarks

Two ways of node numbering different from figure 17 were also applied and in these cases the results were affected by the node allocations according to figure 18. So depending on the way nodes are numbered the numerical tool can become mesh-dependant.

2.5 Thin-walled beam buckling

After validating a simple isotropic beam buckling case, several isotropic beam buckling cases under different boundary conditions and several composite laminated beam cases were compared to closed form solutions.

2.5.1 Case descriptions

An I-shaped beam of length 4000, width 200, height 200 and thickness 18 (figure 16) was chosen for this case. Material properties were chosen according to

table 10.

table 10: material properties

	E_1	E_2	G_{12}	G_{13}	G_{23}	ν_{12}	ν_{21}
isotropic	200000	200000	77000	77000	77000	0.3	0.3
orthotropic	1	$\frac{E_1}{5}$	$\frac{E_2}{2}$	$\frac{E_2}{2}$	$\frac{E_2}{5}$	0.25	$\frac{E_2}{E_1}\nu_{12}$

Nine different cases were distinguished to test the code as can be seen in table 11. Cases 1 to 4 consider different boundary conditions (figure 22 to figure 25), cases 5 to 9 consider different composite laminate layups.

table 11: case descriptions

Case	Boundary conditions	Layup	Figure
1	Left end fixed, right end slider constraint and an applied moment *M*	-	21
2	Both ends hinged, both ends applied moment *M*	-	22
3	Both ends hinged, distributed load *q* applied on top of the beam	-	23
4	Both ends hinged, distributed load *q* applied at the shear centre	-	24
5	Both ends hinged, both ends applied moment *M*	[0]	22
6	Both ends hinged, both ends applied moment *M*	[90]	22
7	Both ends hinged, both ends applied moment *M*	$[0/90]_s$	22
8	Both ends hinged, both ends applied moment *M*	$[0/45/90/-45]_s$	22
9	Both ends hinged, both ends applied moment *M*	$[0/45/-45/90]_s$	22

figure 22

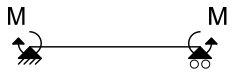

figure 23

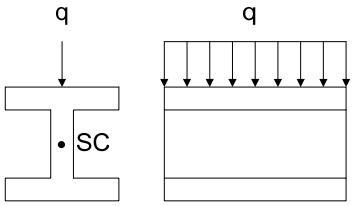

figure 24

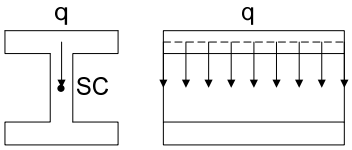

figure 25

2.5.2 Mesh generation

The same mesh as in section 2.4.2 was used.

2.5.3 Boundary conditions

In order to generate hinged and fixed constraints nodes were constrained according to the red arrows shown in figure 26. In order to generate an applied moment forces were applied to nodes according to the green arrows shown in figure 26.

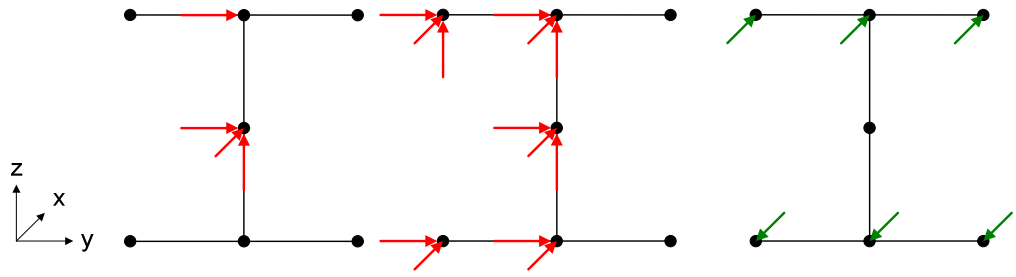

figure 26: hinge constraint, fixed constraint and applied moment

2.5.4 Closed form solutions

In case 1, according to [7] the critical buckling moment can be calculated according to

$$M_{cr} = \frac{\pi}{2L}\sqrt{EI_y GJ_d\left(1 + \frac{\pi^2 EJ_\omega}{4GJ_d L^2}\right)} \tag{6}$$

In case 2, according to [7] critical buckling moment can be calculated according to

$$M_{cr} = \frac{\pi}{L}\sqrt{EI_y GJ_d + \left(\frac{\pi E}{L}\right)^2 I_y J_\omega} \tag{7}$$

In cases 3 and 4, according to [8] the critical distributed buckling force can be calculated according to

$$q_{cr} = \frac{8}{L^2} 1.15 N_{crz}^B \left(0.466f + 0.267\beta_1 + \sqrt{(0.466f + 0.267\beta_1)^2 + \frac{N_{cr\psi}^B i_\omega^2}{N_{crz}^B}} \right) \quad (8)$$

Where f denotes the distance between the shear centre and the applied load and

$$i_\omega^2 = z_{sc}^2 + \frac{EI_y + EI_z}{EA}$$

$$\beta_1 = J_1 + J_2 + 2z_{sc}$$

$$N_{crz}^B = \frac{\pi^2 EI_z}{L^2}$$

$$N_{cr\psi}^B = N_{cr\omega}^B + \frac{GI_t}{i_{\omega^2}}$$

Where z_{sc} denotes the z-coordinate of the shear centre. For the determination of $N_{cr\omega}^B$, J_1 and J_2 please refer to [8]. A second method is also given by [8] and according to this method, the critical distributed buckling force can be calculated according to

$$q_{cr} = \frac{8M_{cr}}{L^2} \quad (9)$$

$$M_{cr} = C_1 \frac{\pi^2}{(kl)^2} \widehat{EI_{zz}} \left(C_2 f + C_3 \beta_1 + \sqrt{(C_2 f + C_3 \beta_1)^2 + \frac{\widehat{EI_\omega}}{\widehat{EI_{zz}}} + \left(1 + \frac{\widehat{GI_t}}{\widehat{EI_\omega}} \frac{(kl)^2}{\pi^2} \right)} \right) \quad (10)$$

Where C_1, C_2 and C_3 depend on the boundary conditions as described in table 13 below. When the rotation of the end cross-sections are not restrained about the z-axis $k = 1$, when these rotations and warping are restrained $k = 0.5$. For the terms $\widehat{EI_{zz}}$, $\widehat{EI_\omega}$ and $\widehat{GI_t}$, please refer to [8].

table 12: constants for Clark and Hill's formula according to [9]

	C_1	C_2	C_3
End moments	1	0	0.5
Uniformly distributed load	1.13	0.45	0.276

2.5.5 Results

All nine cases were run with the numerical tool. The resulting values for the critical applied loads were compared to the closed form solutions and are displayed in table 13 below.

table 13: resulting critical buckling loads

Case no.	Num. tool	(6)	(7)	(8)	(9)	(10)
1	2.780E+08	2.688E+08 (0.0331)	-	-	-	-
2	6.080E+08	-	5.958E+08 (0.0200)	-	-	-
3	2.469E+02	-	-	2.663E+02 (0.0784)	2.639E+02 (0.0690)	-
4	3.214E+02	-	-	3.395E+02 (0.0748)	3.455E+02 (0.0561)	-
5	1.9718E+03	-	-	-	-	2.1137E+03 (0.07198)
6	6.7326E+02	-	-	-	-	6.8684E+02 (0.02016)
7	1.3679E+03	-	-	-	-	1.4408E+03 (0.05332)
8	1.3399E+03	-	-	-	-	1.3754E+03 (0.02652)
9	1.3955E+03	-	-	-	-	1.4456E+03 (0.03588)

2.5.6 Remarks

In these cases lateral-torsional buckling was included in the closed form solutions. Beam dimensions were chosen such that local buckling effects do not (yet) occur.

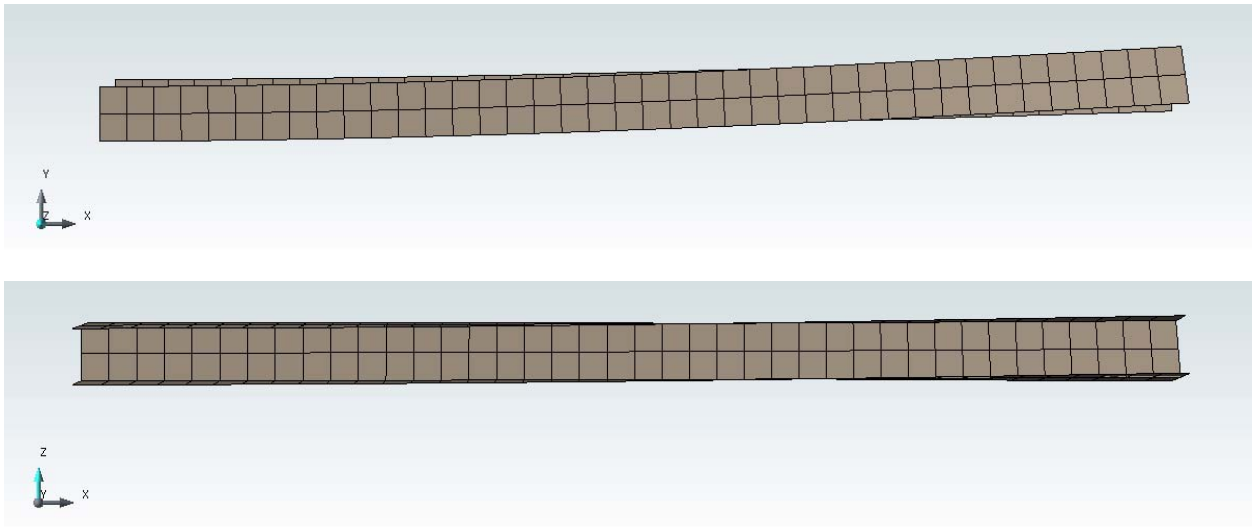

figure 27: lateral torsional buckled shape of case 1

3 Parametric case studies

After making sure the numerical tool yields correct results regarding deflection and buckling behavior of plates and thin-walled structures, several parametric case studies were performed. The first study aims to display the effect of laminate layup on the critical buckling load. The other studies aim to display the effect of beam dimensions on the transition from lateral (figure 27) to local buckling behavior (figure 28).

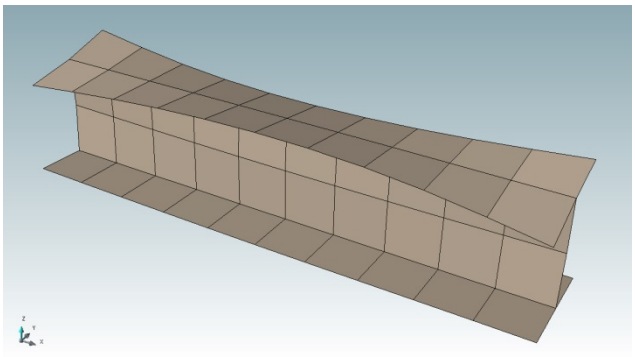

figure 28: local buckling effects

3.1 Effect of laminate layup on critical buckling load

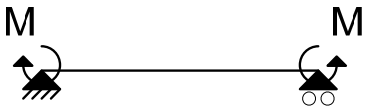

figure 29: a doubly hinged beam under an applied moment at both ends

3.1.1 Case description

A doubly hinged I-shaped beam of length 4000 mm, width 200 mm, height 200 mm and thickness 30 mm (figure 16), under an applied moment M at both ends (figure 29) was chosen for this case. Material properties were chosen according to table 14. The material layup was chosen $[\pm\theta]_{4S}$ where ± denotes two plies: one of orientation θ and one of orientation $-\theta$. θ Ranged from 0 to 90.

table 14: material properties (GPa)

E_1	E_2	G_{12}	G_{13}	G_{23}	ν_{12}	ν_{21}
130.33	7.220	4.230	4.230	4.230	0.337	0.018

3.1.2 Mesh generation

The same mesh as in section 2.4.2 was used.

3.1.3 Boundary conditions

In order to capture the boundary conditions as displayed in figure 29, boundary conditions were applied according to section 2.5.3.

3.1.5 Results

The resulting critical applied moments for a series of θ are shown in table 15 and plotted in graph 1.

table 15: resulting critical moments on an I-shaped

θ	Numerical tool
0	4.09E+08
10	4.53E+08
20	4.74E+08
30	4.29E+08
40	3.57E+08
50	2.75E+08
60	1.98E+08
70	1.37E+08
80	9.09E+07
90	6.88E+07

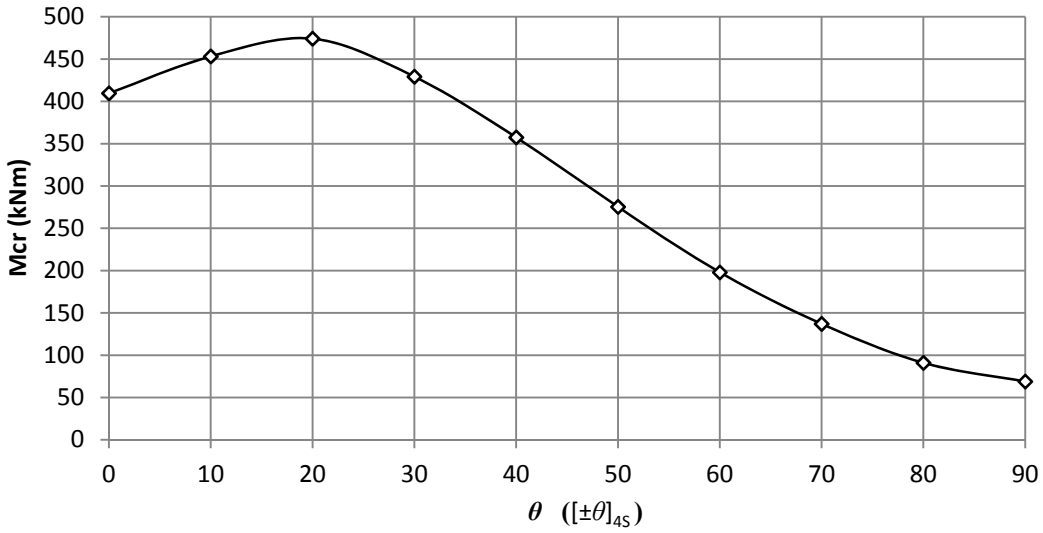

graph 1: critical buckling moments as a function of laminate layup

3.1.6 Remarks

Of course any arbitrary laminate layup may be chosen for the design of a composite laminated thin-walled structure. This study shows the importance of laminate layup when considering a design based on critical buckling loads.

3.2 Transition from lateral to local buckling behavior

3.2.1 Case description

A doubly hinged I-shaped beam of width 200 mm, height 200 mm and thickness 30 mm (figure 16), under an applied moment M at both ends (figure 29) was chosen for this case. Material properties were chosen according to table 14. The material layup was chosen $[0]_{16}$. The beam length ranged from 1000 mm to 5000 mm.

3.2.2 Mesh generation

The same mesh as in section 2.4.2 was used.

3.2.3 Boundary conditions

In order to capture the boundary conditions as displayed in figure 29, boundary conditions were applied according to section 2.5.3.

3.2.4 Closed form solution

In order to determine when local buckling effects start to dominate the buckling behavior, the results of the numerical tool were compared to (10), which assumes lateral beam buckling behavior.

3.2.5 Results

The resulting critical applied moments for a series of beam length L are shown in table 16 and plotted in graph 2.

table 16: resulting critical buckling moments

L	**Numerical tool**	**(10)**
1000	9.947E+08	5.449E+09
2000	9.895E+08	1.451E+09
3000	6.208E+08	7.047E+08
4000	4.095E+08	4.386E+08
5000	2.985E+08	3.116E+08

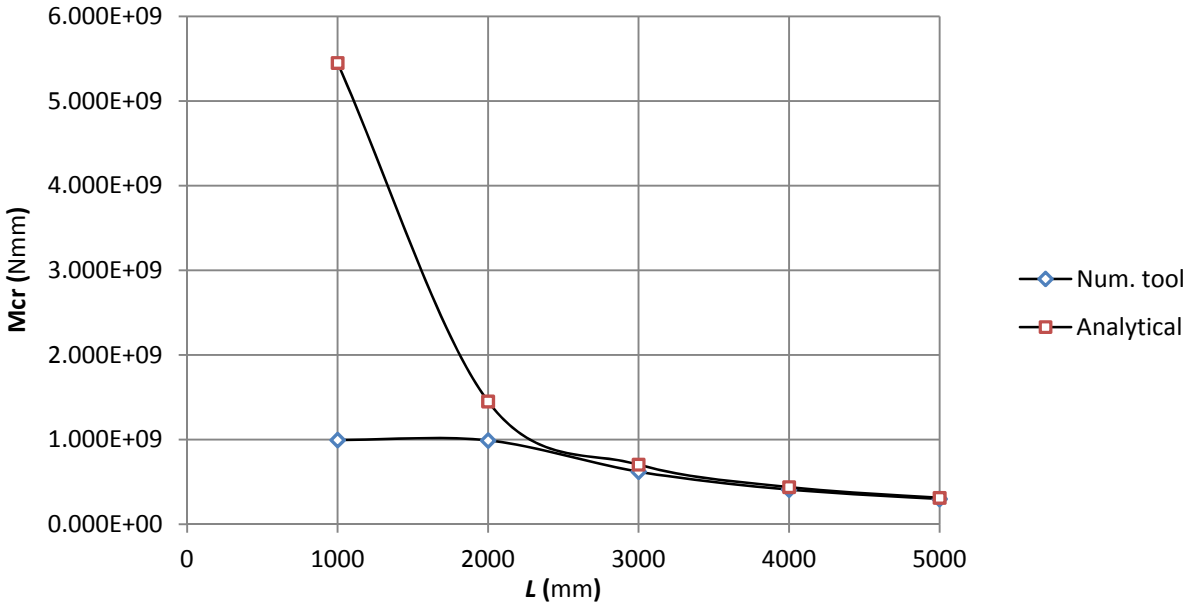

graph 2: critical buckling moment as a function of beam length

3.2.6 Remarks

This study clearly shows that for short beams, local buckling effects start to dominate the buckling behavior. Of course many other parameters such as cross-sectional dimensions and laminate layup determine the transition from lateral to local buckling behavior. A same study has been performed with varying beam thickness and for relatively thin beams local buckling effects dominate buckling behavior (graph 3). This study shows that through the use of shell elements, local buckling effects can be captured.

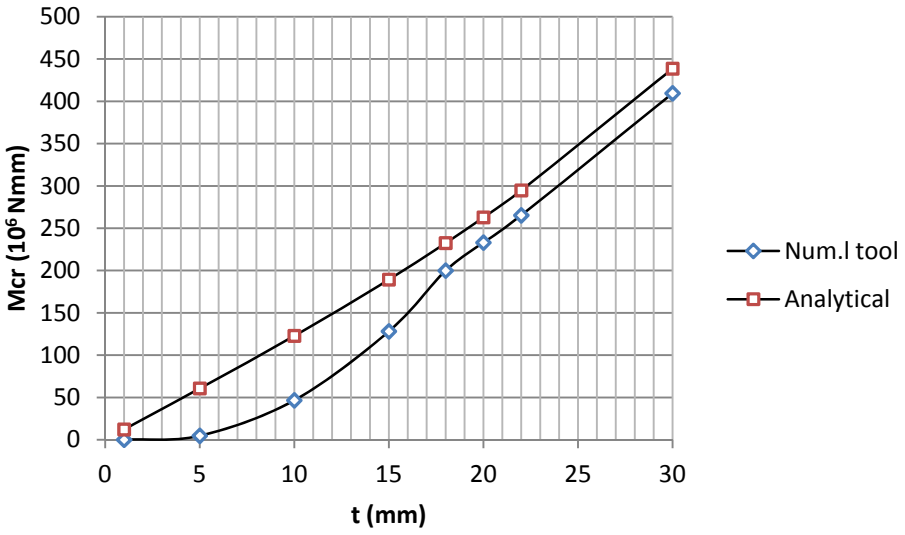

graph 3: critical buckling moment as a function of beam thickness

4 Convergence studies

The parametric case studies and validation were performed with a shell element named shell element 2. Two other types of shell elements were incorporated into the code, named shell element 1 and shell element 3. Shell element 1 is the simplest shell element, but quite prone to locking. Shell element 2 uses selective reduced integration to prevent locking. Shell element 3 was based on the twist-Kirchhoff theory according to [2] and supposedly has a superior convergence rate. However, according to [2] in order for the shell element to perform optimally the mesh has to meet certain conditions (as explained in section 4.1). Several convergence studies were performed in order to compare these three elements.

4.1 Mesh conditions for twist-Kirchhoff shell element

As mentioned in chapter one, each element has four nodes and each node is given six degrees of freedom. For normal mesh conditions we assume that nodes of neighboring elements are tied in all six degrees of freedom because elements share nodes. For example, in figure 30 node b and e are tied in all six degrees of freedom because node b *is* node e. Subsequently, node c, h, j and m are all the same node and are thus tied in all degrees of freedom.

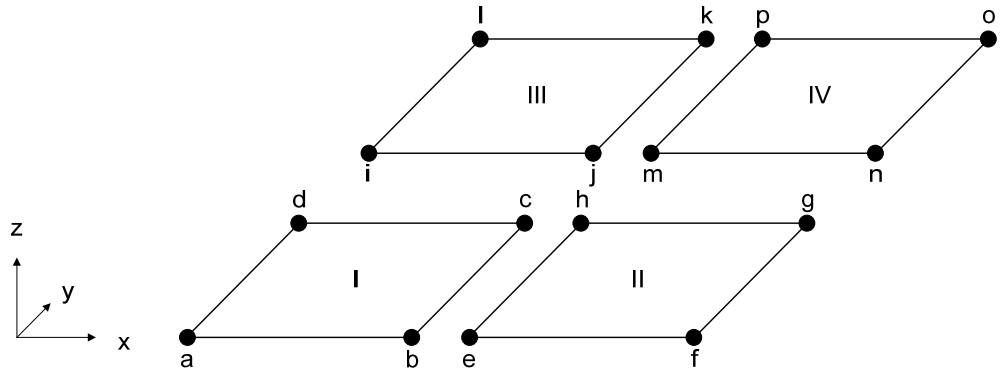

figure 30: nodal ties amongst 4 elements

However, shell element 3 requires that the mesh releases certain degrees of freedom between certain nodes. The condition states that on the boundary between two neighboring elements, the rotation over the axis perpendicular to the boundary is released. For example, in figure 30 node b and e should not be tied in the rotation about the x-axis. Node c and h should also not be tied in the rotation about the x-axis. Node d and i, as well as node c and j should be uncoupled in their rotation about the y-axis. Etc..

The publishing ([2]) is not clear on how this mesh-condition should be realized. For these studies so called MPC-constraints were chosen. MPC constraints state that one node (slave-node) becomes tied to another node (master-node) in a certain degree of freedom. Despite a supposedly superior convergence rate for shell element 3, stating 5 MPC constraints per node becomes computationally very expensive and implicates the mesh generation process considerably.

4.2 Convergence studies on square plates

4.2.1 Case descriptions

A thin square plate of length 1, width 1 and thickness either 0.01 or 0.001 was chosen for this case. The plate was chosen to be either simply supported or clamped along the edges. Plate deflection due to a central point load (figure 9) and plate buckling due to biaxial compression (figure 13) were chosen for the loading types. Table 17 summarizes the 8 cases that were chosen for the convergence studies.

table 17: case descriptions

Case no.	t	Boundary conditions	loading
1	0.01	Simply supported	Central point load
2	0.001	Simply supported	Central point load
3	0.01	Clamped edges	Central point load
4	0.001	Clamped edges	Central point load
5	0.01	Simply supported	Biaxial compression
6	0.001	Simply supported	Biaxial compression
7	0.01	Clamped edges	Biaxial compression
8	0.001	Clamped edges	Biaxial compression

Material properties were chosen according to table 18 below.

table 18: material properties

E_1	E_2	G_{12}	G_{13}	G_{23}	ν_{12}	ν_{21}
10000000	10000000	3846154	3846154	3846154	0.3	0.3

4.2.2 Mesh generation

Meshes of 2x2, 4x4, 8x8 and 16x16 elements were generated for each case and nodes were numbered according to figure 10. Elements were assigned a thickness value of either 0.01 or 0.001 according to table 17.

4.2.3 Boundary conditions

For cases 1,2 and 3,4 boundary conditions were applied to sections 2.2.3 and 2.3.3 respectively. For cases 3,4 and 5,6 boundary conditions were applied to sections 2.2.3 and 2.3.3 respectively as well, except that rotations about the edges were now restricted as shown in figure 31.

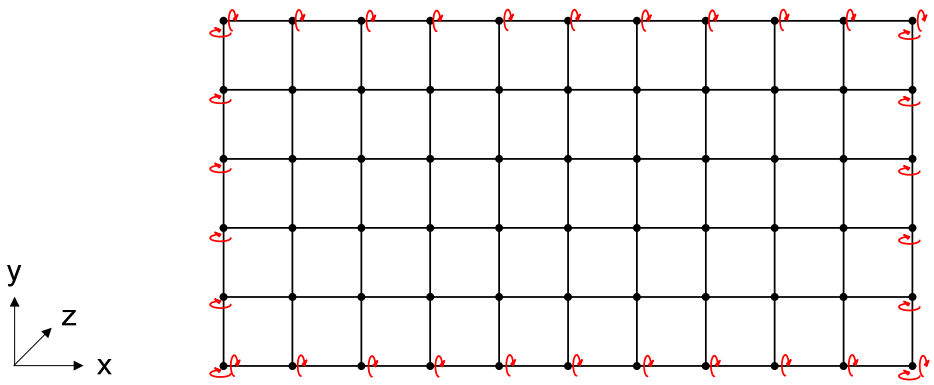

figure 31: added constraints for the clamped edge boundary condition

4.2.4 Closed form solutions

Cases 1 and 2 were compared to (3). Cases 5 and 6 were compared to (5). Cases 3 and 4 can be compared to

$$\omega_0 = 0.005612\frac{Pa^2}{D} \tag{11}$$

where

$$D = \frac{Et^3}{12(1-\nu^2)}$$

Unfortunately, no closed form solution was found to compare cases 7 and 8 to.

4.2.5 Results

After running each case with a mesh of 2x2, 4x4, 8x8 and 16x16 elements the resulting maximum displacements resp. critical buckling loads were plotted against the number of elements in graph 4 to graph 11.

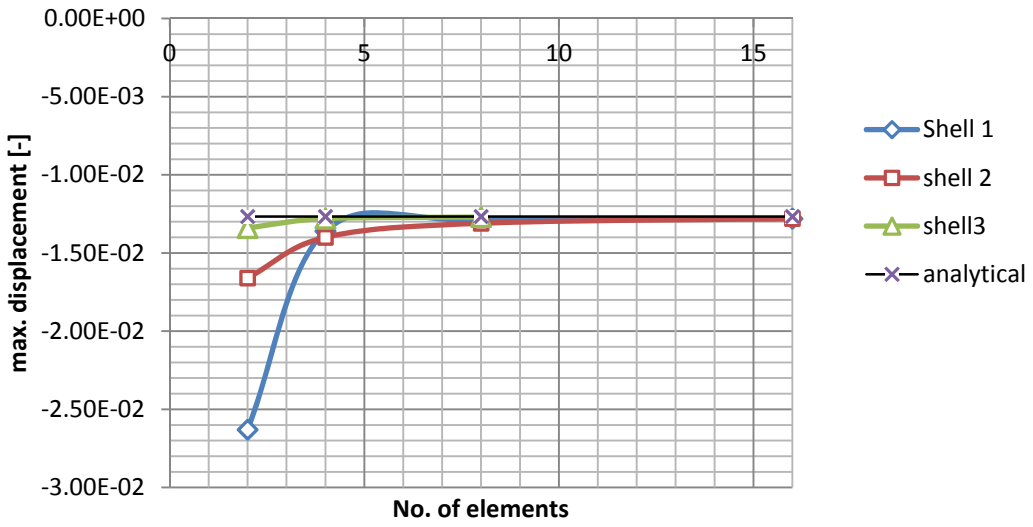

graph 4: maximum displacement plotted against number of elements per side for case 1

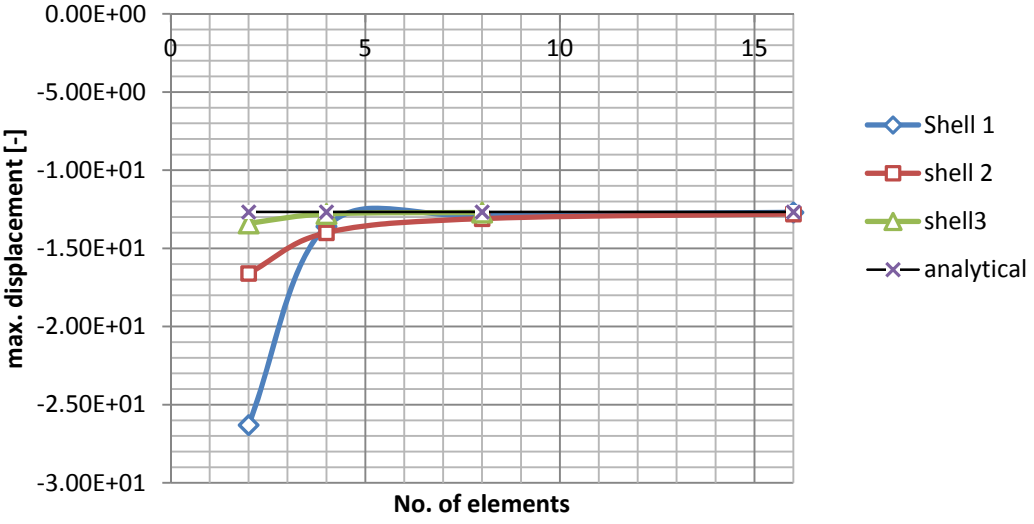

graph 5: maximum displacement plotted against number of elements per side for case 2

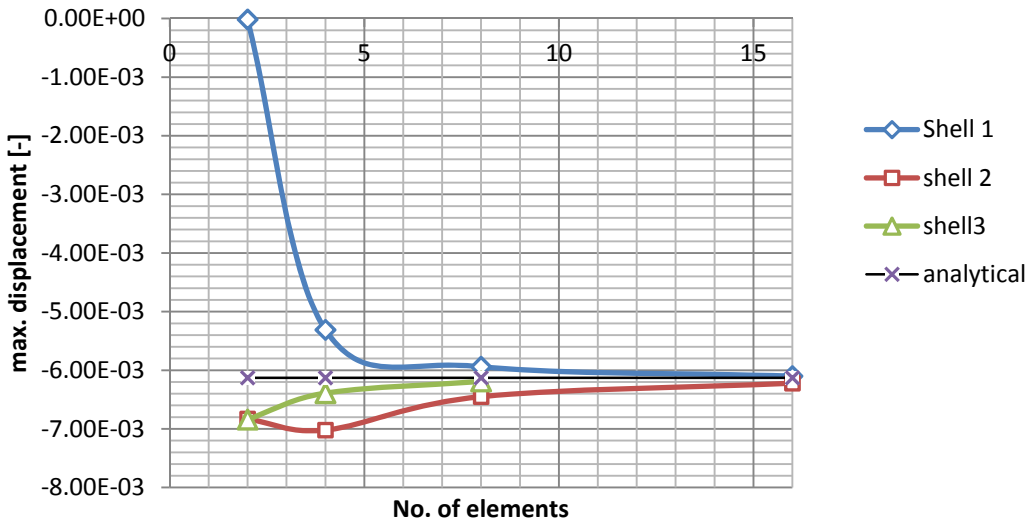

graph 6: maximum displacement plotted against number of elements per side for case 3

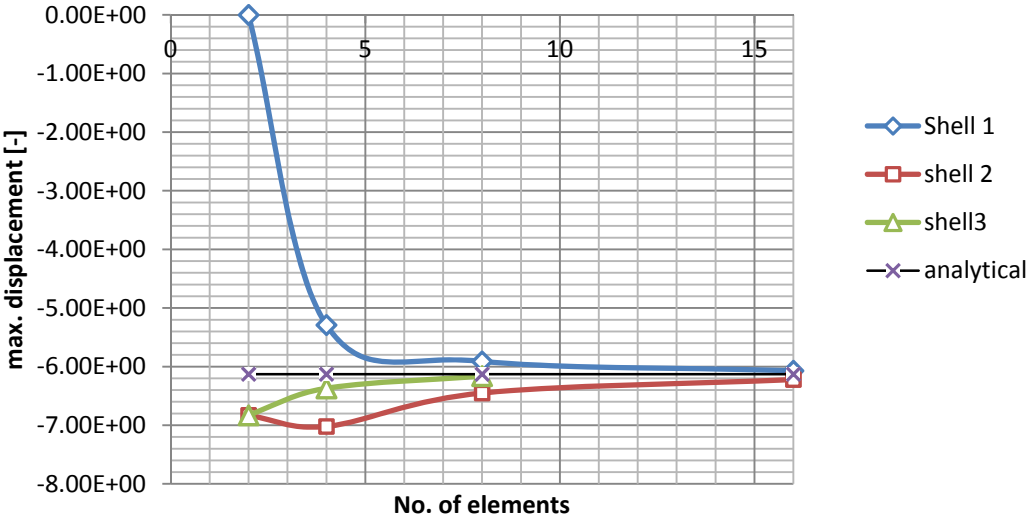

graph 7: maximum displacement plotted against number of elements per side for case 4

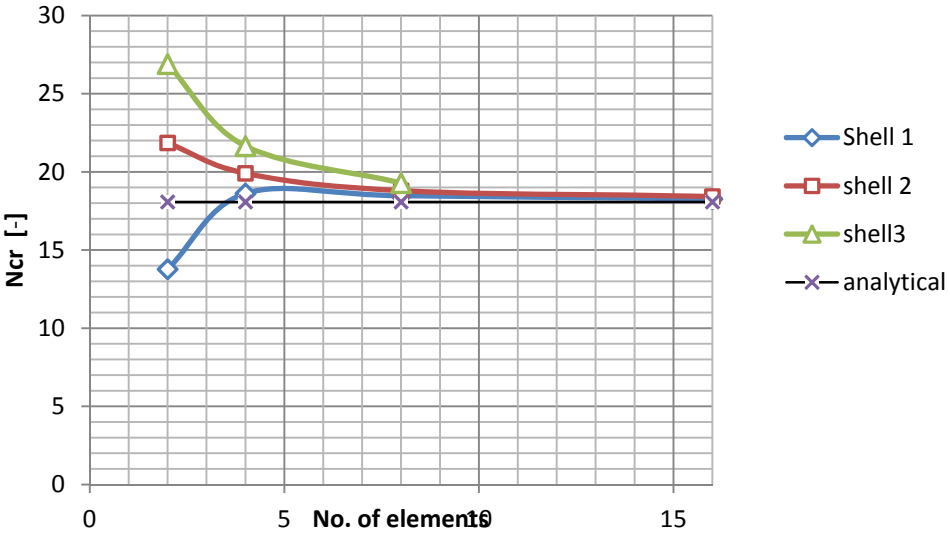

graph 8Critical buckling load plotted against number of elements per side for case 5

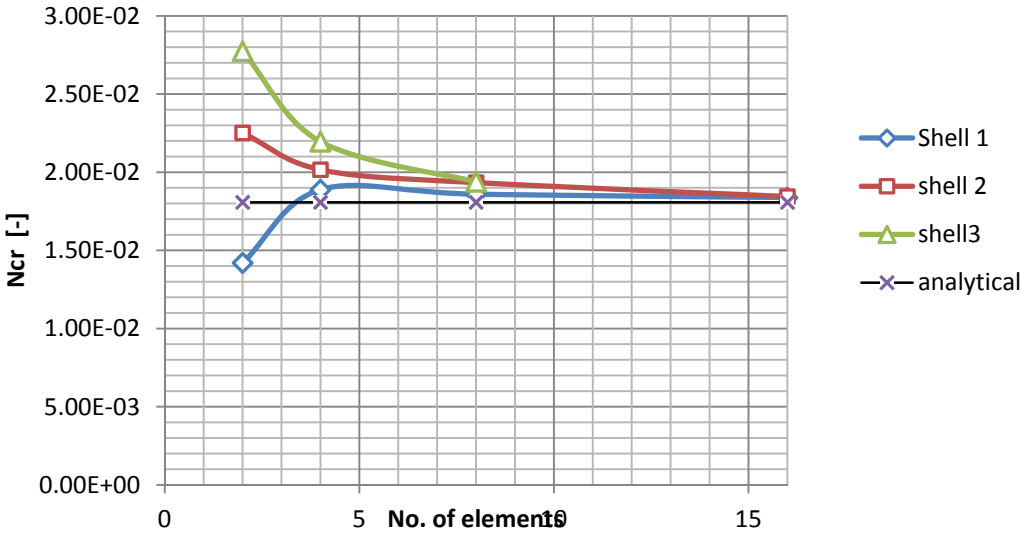

graph 9: Critical buckling load plotted against number of elements per side for case 6

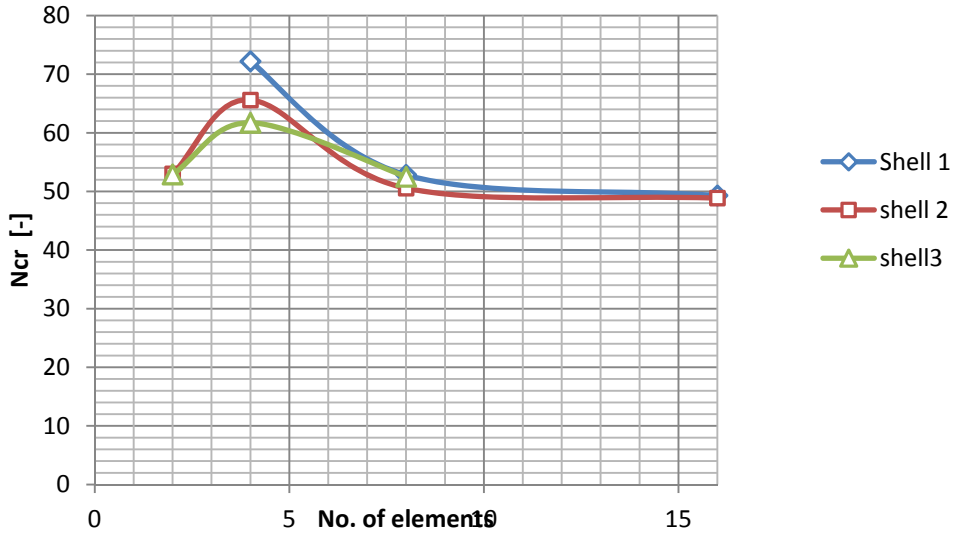

graph 10: Critical buckling load plotted against number of elements per side for case 7

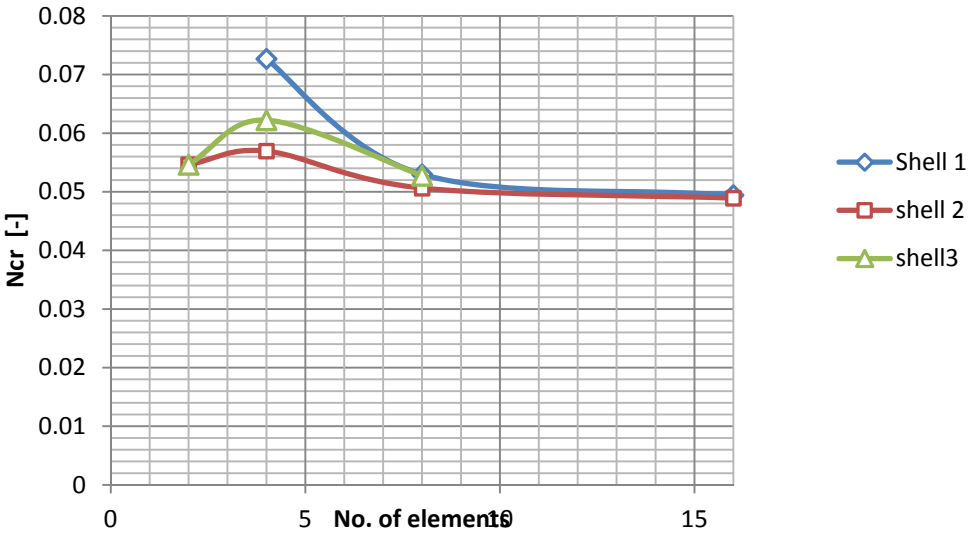

graph 11: Critical buckling load plotted against number of elements per side for case 8

5 Conclusions

From chapter 2, where the validation was performed with a shell element based on selective reduced integration (shell element 2) we can conclude that the tool generally performs adequately. However, for the case of non-square plate deflections the error made was unacceptably large and no explanation for this was found. In the case of non-square plate buckling the error was very large but can be explained by the closed form's assumption on the buckled shape.

From chapter 3 we can conclude that laminate properties play an important role in the critical buckling loads of thin-walled beams and could even cause a transition from global to local buckling effects. Chapter 3 also illustrates that the assumption of lateral buckling behavior is not valid for any arbitrary thin-walled beam.

Although the numerical tool is computationally quite expensive, the method can clearly calculate correct critical applied loads. Perhaps a homogenization can be applied within the current commercially available software in order to provide more accurate results. Perhaps other ways can be thought of to include this numerical tool in order to consider local buckling effects.

From chapter 4 we can conclude that in the case of thin plate deflections, shell elements based on the twist-Kirchhoff theory (shell element 3) provide superior convergence compared to shell elements based on selective reduced integration (shell element 2). However for the case of thin plate buckling (and possibly thin-walled beam buckling) shell element 3 has no superior convergence rate. Due to the fact that mesh generation and computing time become very expensive it would not be advisable to apply shell element 3 to buckling problems.

Bibliography

[1] R. E. Erkmen, B.A. Göttgens, "Buckling analysis of thin-walled composite laminated members using a new shell element" *Composite Structures*, not yet published

[2] F. Brezzi, J.A. Evans, T.J.R Hughes, L.D. Marini, "New rectangular plate elements based on twist-Kirchhoff theory", *Comput. Methods Appl. Mech. Engrg.* 200 (2011) 2547–2561

[3] J.N. Reddy, "Mechanics of laminated composite plates and shells: Theory and Analysis", 2nd ed., *CRC Press* (2003) 202-209

[4] S.P. Timoshenko, S. Woinowsky-Krieger, "Theory of Plates and Shells, 2nd ed", *McGraw-Hill, New York, NY* (1959)

[5] J.N. Reddy, "Mechanics of laminated composite plates and shells: Theory and Analysis", 2nd ed., *CRC Press* (2003) 247-249

[6] S.P. Timoshenko, S. Woinowsky-Krieger, "Theory of Plates and Shells, 2nd ed", *McGraw-Hill, New York, NY* (1959) 432

[7] R.E. Erkmen, M. Mohareb, " Buckling analysis of thin-walled open members – A finite element formulation", *Thin-Walled Structures* 46 (2008) 618–636

[8] A. Sapkás, L.P. Kollár, "Lateral-torsional buckling of composite beams", *International Journal of Solids and Structures* 39 (2002) 2939–2963

[9] N.S. Trahair, "Flexural–torsional buckling of structures" *Boca Raton, FL, USA: CRC Press* (1993)

Appendix 1 Derivation of stiffness matrices

Constitutive relations

For a laminate composed of n orthotropic layers, with their local xy-plane oriented arbitrarily with respect to the global xy-plane whose orientation is determined by angle ϕ which is the clock-wise angle about the Z-axis from the laminate coordinates XYZ to material coordinates $X_1X_2X_3$, the stress-strain relationship for the k^{th} layer can be written as

$$\boldsymbol{\sigma}^{(k)} = \begin{Bmatrix} \sigma_x^{(k)} \\ \sigma_y^{(k)} \\ \tau_{xy}^{(k)} \end{Bmatrix} = \bar{\mathbf{Q}}^{(k)}\boldsymbol{\varepsilon}$$

where

$$\bar{\mathbf{Q}}^{(k)} = \begin{bmatrix} \bar{Q}_{11}^{(k)} & \bar{Q}_{12}^{(k)} & \bar{Q}_{16}^{(k)} \\ \bar{Q}_{12}^{(k)} & \bar{Q}_{22}^{(k)} & \bar{Q}_{26}^{(k)} \\ \bar{Q}_{16}^{(k)} & \bar{Q}_{26}^{(k)} & \bar{Q}_{66}^{(k)} \end{bmatrix},$$

where

$$\bar{Q}_{11}^{(k)} = Q_{11}^{(k)}\cos^4\phi_k + 2\left(Q_{12}^{(k)}+2Q_{66}^{(k)}\right)\sin^2\phi_k\cos^2\phi_k + Q_{22}^{(k)}\sin^4\phi_k$$

$$\bar{Q}_{12}^{(k)} = \left(Q_{11}^{(k)} + Q_{22}^{(k)} - 4Q_{66}^{(k)}\right)\sin^2\phi_k\cos^2\phi_k + Q_{12}^{(k)}\left(\sin^4\phi_k + \cos^4\phi_k\right)$$

$$\bar{Q}_{22}^{(k)} = Q_{11}^{(k)}\sin^4\phi_k + 2\left(Q_{12}^{(k)}+2Q_{66}^{(k)}\right)\sin^2\phi_k\cos^2\phi_k + Q_{22}^{(k)}\cos^4\phi_k$$

$$\bar{Q}_{16}^{(k)} = \left(Q_{11}^{(k)} - Q_{12}^{(k)} - 2Q_{66}^{(k)}\right)\sin\phi_k\cos^3\phi_k + \left(Q_{12}^{(k)} - Q_{22}^{(k)} + 2Q_{66}^{(k)}\right)\sin^3\phi_k\cos\phi_k$$

$$\bar{Q}_{26}^{(k)} = \left(Q_{11}^{(k)} - Q_{12}^{(k)} - 2Q_{66}^{(k)}\right)\sin^3\phi_k\cos\phi_k + \left(Q_{12}^{(k)} - Q_{22}^{(k)} + 2Q_{66}^{(k)}\right)\sin\phi_k\cos^3\phi_k$$

$$\bar{Q}_{66}^{(k)} = \left(Q_{11}^{(k)} + Q_{22}^{(k)} - 2Q_{12}^{(k)} - 2Q_{66}^{(k)}\right)\sin^2\phi_k\cos^2\phi_k + Q_{66}^{(k)}\left(\sin^4\phi_k + \cos^4\phi_k\right)$$

$$\bar{Q}_{44}^{(k)} = Q_{44}^{(k)}\cos^2\phi_k + Q_{55}^{(k)}\sin^2\phi_k$$

$$\bar{Q}_{45}^{(k)} = \left(Q_{55}^{(k)} - Q_{44}^{(k)}\right)\cos\phi_k\sin\phi_k$$

$$\bar{Q}_{55}^{(k)} = Q_{44}^{(k)}\sin^2\phi_k + Q_{55}^{(k)}\cos^2\phi_k$$

in which

$$Q_{11}^{(k)} = \frac{E_1^{(k)}}{1-\upsilon_{12}^{(k)}\upsilon_{21}^{(k)}},$$

$$Q_{12}^{(k)} = \frac{\upsilon_{12}^{(k)}E_2^{(k)}}{1-\upsilon_{12}^{(k)}\upsilon_{21}^{(k)}},$$

$$Q_{22}^{(k)} = \frac{E_2^{(k)}}{1-\upsilon_{12}^{(k)}\upsilon_{21}^{(k)}},$$

$$Q_{66}^{(k)} = G_{12}^{(k)},$$

$$Q_{44}^{(k)} = G_{23}^{(k)},$$

$$Q_{55}^{(k)} = G_{13}^{(k)},$$

where $E_1^{(k)}$, $E_2^{(k)}$ Young's moduli of the k^{th} layer in the local x (1) and y (2) (principal) directions of the material (coordinates), respectively, $G_{12}^{(k)}$, $G_{13}^{(k)}$ and $G_{23}^{(k)}$ are shear moduli in the 1-2, 1-3 and 2-3 planes of the k^{th} layer, $\upsilon_{ij}^{(k)}$ is the Poisson's ratio defined as the ratio of the transverse strain in the j^{th} direction to the axial strain in i^{th} direction.

Stress resultants

It is customary to associate the stresses with moments and forces per unit length in x-y plane. The stress resultant vector of membrane forces in x-y -plane can be written as

$$\mathbf{N} = \begin{Bmatrix} N_x & N_y & N_{xy} \end{Bmatrix}^{\mathrm{T}} = \sum_{k=1}^{n}\left(\int_{z_k}^{z_{k+1}} \boldsymbol{\sigma}^{(k)}\mathrm{d}z\right) = \sum_{k=1}^{n}\left(\int_{z_k}^{z_{k+1}} \bar{\mathbf{Q}}^{(k)}\boldsymbol{\varepsilon}\mathrm{d}z\right) = \mathbf{A}\left(\boldsymbol{\varepsilon}_m + \boldsymbol{\varepsilon}_N\right) + \mathbf{B}\boldsymbol{\chi},$$

where

$$\mathbf{A} = \begin{bmatrix} A_{11} & A_{12} & A_{16} \\ A_{12} & A_{22} & A_{26} \\ A_{16} & A_{26} & A_{66} \end{bmatrix},$$

in which

$$A_{ij} = \sum_{k=1}^{n} \bar{Q}_{ij}^{(k)} \left(Z_k - Z_{k-1} \right), \qquad (i, j = 1,2,6)$$

The vector of bending moments M_x and M_y in *x*-*z* and in *y*-*z* –planes, respectively and the twisting moment M_{xy} can be written as

$$\mathbf{M} = \left\langle M_x \quad M_y \quad M_{xy} \right\rangle^{\mathrm{T}} = \sum_{k=1}^{n} \left(\int_{z_k}^{z_{k+1}} \boldsymbol{\sigma}^{(k)} z \, \mathrm{d}z \right) = \sum_{k=1}^{n} \left(\int_{z_k}^{z_{k+1}} \bar{\mathbf{Q}}^{(k)} \boldsymbol{\varepsilon} z \, \mathrm{d}z \right) = \mathbf{B}\left(\boldsymbol{\varepsilon}_m + \boldsymbol{\varepsilon}_N \right) + \mathbf{D}\boldsymbol{\chi} \quad (1)$$

where

$$\mathbf{B} = \begin{bmatrix} B_{11} & B_{12} & B_{16} \\ B_{12} & B_{22} & B_{26} \\ B_{16} & B_{26} & B_{66} \end{bmatrix},$$

in which

$$B_{ij} = \frac{1}{2} \sum_{k=1}^{n} \bar{Q}_{ij}^{(k)} \left({Z_k}^2 - {Z_{k-1}}^2 \right), \quad (i, j = 1,2,6)$$

and

$$\mathbf{D} = \begin{bmatrix} D_{11} & D_{12} & D_{16} \\ D_{12} & D_{22} & D_{26} \\ D_{16} & D_{26} & D_{66} \end{bmatrix}$$

in which

$$D_{ij} = \frac{1}{3} \sum_{k=1}^{n} \bar{Q}_{ij}^{(k)} \left({Z_k}^3 - {Z_{k-1}}^3 \right) \quad (i, j = 1,2,6)$$